International Journal of Thermal Sciences 48 (2009) 1116–1128

Contents lists available at ScienceDirect

International Journal of Thermal Sciences

www.elsevier.com/locate/ijts

Numerical analysis of solidification of a 3-D semitransparent medium in presence of volumetric radiation

Bittagopal Mondal, Subhash C. Mishra *

Department of Mechanical Engineering, Indian Institute of Technology Guwahati, Guwahati 781039, India

ARTICLE INFO

Article history:
Received 5 April 2008
Received in revised form 8 October 2008
Accepted 8 October 2008
Available online 30 October 2008

Keywords:
Radiation
Conduction
Semitransparent medium
Solidification
Lattice Boltzmann method
Finite volume method

ABSTRACT

Solidification of a 3-D cubical semitransparent absorbing, emitting and scattering semitransparent medium in the presence of volumetric radiation is analyzed. An enthalpy based lattice Boltzmann method is used to analyze the solidification process. Radiative information is computed using the finite volume method. Over a range of temperatures, a distinct liquid-, mushy- and solid-zones are considered. Cases of both Dirichlet and Neumann boundary conditions are taken up. Liquid fraction and temperature distributions in the medium are analyzed for the effects of the extinction coefficient, the scattering albedo, the conduction-radiation parameter and the latent heat.

1. Introduction

Mathematical modeling of phase change of semitransparent materials is an important field of research. It has relevance in various engineering applications such as films used in solar energy, crystal growth, alloy processing, nuclear engineering and laser material processing [1–15]. Semitransparent materials such as oxides, fluorides and silicon find applications as single- and poly-crystals, glasses, ceramics, composites, etc. [16–21].

One of the early numerical studies of melting and solidification has been reported by Co and Sunderland [1]. Habib [2] considered solidification of semitransparent materials. In his study, he considered the effects of conduction and radiation. Abrams and Viskanta [3] considered effects of radiative heat transfer in melting and solidification of semitransparent crystals. Effects of scattering on melting and solidification of a semi-infinite semitransparent medium was taken into account by Oruma et al. [4]. Morphological stability during directional solidification due to radiative heat transfer was analyzed by Yuferev et al. [5]. Shu et al. [6] studied effects of internal radiation and solidification in semitransparent melts in the presence of magnetic fields.

In the presence of volumetric radiation, solidifications of 1-D planar and 2-D square geometries were analyzed by Raj et al. [7] and Mishra et al. [8]. In [7,8], the lattice Boltzmann method (LBM) [22–30] was used to analyze the solidification process. The discrete transfer method was applied to compute radiation information in case of a 1-D planar medium in [7]. In [8], in case of a 2-D square geometry, the finite volume method (FVM) was used to compute the radiative information.

Chatterjee and Chakraborty [9–11] have formulated an enthalpy based lattice Boltzmann model for the simulation of melting of a 3-D cubical medium. De Fabritiis et al. [13] and Miller et al. [14] are the proponents who used the LBM formulation to analyze phase-change problems. However, the analyses presented in [9–14] were limited to materials which did not require consideration of volumetric radiation.

From the literature review it has been found that none of the studies reported so far has analyzed solidification of a 3-D semitransparent medium considering effects of volumetric radiation. The present work, therefore, is aimed at the analysis of solidification of a 3-D absorbing, emitting and scattering semitransparent medium involving radiation. An enthalpy based formulation in the LBM [22–30] is employed to simulate the solidification process. Solidification is assumed to take place over a range of temperatures, and accordingly distinct liquid-, mushy- and solid-zones are considered. The FVM [31,32] is used to compute the radiative information. Analyses are done considering both Dirichlet and Neumann boundary conditions. The liquid fraction and temperature profiles in the medium are analyzed for the effects of various parameters such as the extinction coefficient, the scattering albedo, the conduction-radiation parameter and the latent heat.

* Corresponding author. Tel.: +91 361 2582660; fax: +91 361 2690762.
E-mail address: scm_iitg@yahoo.com (S.C. Mishra).

1290-0729/$ – see front matter
doi:10.1016/j.ijthermalsci.2008.10.001

Nomenclature

A	area	m^2
b	number of directions in a lattice	
c_P	specific heat	kJ/kg K
C	heat capacity	kJ/m^3 K
$\vec{e}_i$	propagation velocity in the direction i in the lattice	m/s
f_l	volume phase fraction of the liquid phase	
G	incident radiation	W/m^2
H	total enthalpy	kJ/kg
I	intensity	W/m^2
k	thermal conductivity	W/m K
L	latent heat	kJ/kg
M	total number of rays/intensities	
N	conduction-radiation parameter	
n_i	particle distribution function in the i-direction	K
$n_i^{(0)}$	equilibrium particle distribution function in the i-direction	K
q_R	radiative heat flux	W/m^2
$\vec{r}$	lattice node	m
S	radiative source term	W/m^2
T	temperature	K
t	time	s
V	volume	m^3
w_i	weight factor corresponding to the direction i in a lattice	
X, Y, Z	x-, y- and z-dimensions of the geometry	m
x, y, z	coordinate directions	

Greek symbols

α	thermal diffusivity	m^2/s
β	extinction coefficient	m^{-1}
ε	emissivity	
ρ	density	kg/m^3
θ	polar angle	
ϕ	azimuthal angle	
σ	Stefan–Boltzmann constant	
τ	relaxation time	s
$\Delta\Omega$	elemental solid angle	
ω	scattering albedo	
Φ	source term which affects the distribution function n_i, Eq. (24)	

Subscript

b	boundary
E, W, N, S, F, B	east, west, north, south, front and back
i	lattice direction index
0	initial temperature
l	liquid phase
f	freezing
P	cell center
s	solid phase

Superscript

0	equilibrium
m	direction index

2. Formulation

Solidification of a 3-D cubical (Fig. 1a) semi-transparent absorbing, emitting and scattering medium is considered. Initially at time $t = 0$, the liquid pool is at temperature T_0. The freezing temperature of the material is T_f which is lower than the initial temperature T_0. For time $t > 0$, the north boundary and south boundary are maintained at temperatures T_N and T_S, respectively. These temperatures are below its freezing temperature T_f. The remaining four boundaries are maintained at the initial temperature T_0. Since temperatures of the north and south boundaries are lower than the freezing temperature of the material, the solidification starts from these boundaries. Prior to solidification, a mushy zone appears within the material. For the material under consideration, solidification is considered over a range of temperatures. Since the material is semitransparent, thermal radiation pervades the material and its consideration becomes paramount in the energy equation.

For the problem under consideration, energy equation with volumetric radiation in terms of total enthalpy can be written as

$$\frac{\partial(\rho H)}{\partial t} = \nabla\cdot(k\nabla T) - \nabla\cdot\vec{q}_R \tag{1}$$

where ρ is the density, H is the total enthalpy, k is the thermal conductivity, T is the temperature and $\vec{q}_R$ is the radiative heat flux.

In Eq. (1), the total enthalpy H consists of two parts i.e. sensible enthalpy $c_P T$ and latent enthalpy $f_l L$. c_P is the specific heat at constant pressure, f_l is the liquid fraction and L is the latent heat of fusion. Different zones, viz. solid-, liquid- and mushy-zones are identified with the values of the liquid fraction f_l. For liquid-zone, $f_l = 1$. If $f_l = 0$, then it is a solid-zone and for the mushy-zone, $0 < f_l < 1$. Using the definition of the total enthalpy $H = c_P T + f_l L$, the energy equation is written as

$$\frac{\partial(\rho c_P T)}{\partial t} = \nabla\cdot(k\nabla T) - L\frac{\partial(\rho f_l)}{\partial t} - \nabla\cdot\vec{q}_R \tag{2}$$

If ρ, c_P and k are assumed constant over a particular zone and also independent of time, Eq. (2) for a specific zone (solid-, mushy- and liquid) can be written as

$$\frac{\partial T}{\partial t} = \alpha\nabla^2 T - \frac{L}{C}\frac{\partial(\rho f_l)}{\partial t} - \frac{1}{C}\nabla\cdot\vec{q}_R \tag{3}$$

where $\alpha = k/\rho c_P$ is the thermal diffusivity and $C = \rho c_P$ is the heat capacity. In the solid-, mushy- and liquid-zones, the liquid fraction f_l and enthalpy are related as

$$f_l = \begin{cases} 0, & H < H_s \\ \frac{H-H_s}{H_l-H_s}, & H_s \leqslant H \leqslant H_l \\ 1, & H > H_l \end{cases} \tag{4}$$

In Eq. (4), subscripts s and l stand for solid- and liquid-zones, respectively. The enthalpy based energy equation (3) can be solved by any of the conventional CFD tools, such as the FVM.

Recently solidification problems have also been analyzed by the LBM [7–9,11,12,26]. Jiaung et al. [26], Raj et al. [7], Mishra et al. [8] and Chatterjee and Chakraborty [9,11,12] have used the LBM to analyze phase change problems. Like fluid dynamics, use of the LBM is also gaining momentum in solving heat transfer problems [7,8,11–14,26–30]. Proponents [13,14,22–25] of the LBM claim that this method has the potential to be a robust CFD platform. In the present work, therefore, we analyze the 3-D solidification problem using the LBM.

The FVM for computation of radiative information is a robust method [31,32]. Because of its construction, the method is fully conservative. In [30], compatibility of the LBM and FVM for solving

conduction-radiation problems in 1-D and 2-D Cartesian geometries has been demonstrated. In the present work, therefore, the solidification problem which is analyzed by the LBM, the radiative information is computed using the FVM.

In the following sections, first we describe a brief formulation of FVM to compute the radiative heat flux $\nabla \cdot \vec{q}_R$ followed by the LBM formulation to simulate the phase transition process.

2.1. Finite Volume Method (FVM)

The radiative transfer equation in any discrete direction $\hat{s}^m = (\sin\theta^m \cos\phi^m)\hat{i} + (\sin\theta^m \sin\phi^m)\hat{j} + (\cos\theta^m)\hat{k}$ with direction index m is given by [31,32]

$$\frac{dI^m}{ds^m} = -\beta I^m + S^m \tag{5}$$

where I is the intensity and β is the extinction coefficient. The source term S for an absorbing, emitting and isotropically scattering medium is given by

$$S = \beta(1-\omega)\left(\frac{\sigma T^4}{\pi}\right) + \frac{\beta\omega}{4\pi}G \tag{6}$$

where $\omega = \sigma_s/\beta$ is the scattering albedo.

Resolving Eq. (5) along the x-, y- and z-coordinate directions and integrating it over the elemental solid-angle $\Delta\Omega^m$, we get

$$\frac{\partial I^m}{\partial x}D_x^m + \frac{\partial I^m}{\partial y}D_y^m + \frac{\partial I^m}{\partial z}D_z^m = -\beta I^m \Delta\Omega^m + S^m \Delta\Omega^m \tag{7}$$

If $\hat{n}$ is the outward normal to a surface, then D^m is given by

$$D^m = \int_{\Delta\Omega^m} (\hat{n}\cdot\hat{s}^m)\, d\Omega \tag{8}$$

When the outward normal $\hat{n}$ is pointing towards one of the positive coordinate directions, D_x^m, D_y^m and D_z^m are given by [29]

$$D_x^m = \cos\phi^m \sin\left(\frac{\Delta\phi^m}{2}\right)\left[\Delta\theta^m - \cos 2\theta^m \sin(\Delta\theta^m)\right] \tag{9}$$

$$D_y^m = \sin\phi^m \sin\left(\frac{\Delta\phi^m}{2}\right)\left[\Delta\theta^m - \cos 2\theta^m \sin(\Delta\theta^m)\right] \tag{10}$$

$$D_z^m = \sin\theta^m \cos\theta^m \sin(\Delta\theta^m)\Delta\phi^m \tag{11}$$

For $\hat{n}$ pointing towards the negative coordinate directions, signs of D_x^m, D_y^m and D_z^m are opposite to what are obtained from Eqs. (9)–(11). In Eq. (7), $\Delta\Omega^m$ is given by

$$\Delta\Omega^m = 2\sin\theta^m \sin\left(\frac{\Delta\theta^m}{2}\right)\Delta\phi^m \tag{12}$$

Integrating Eq. (7) over a 3-D control volume, we get

$$\left[I_E^m - I_W^m\right]A_x D_x^m + \left[I_N^m - I_S^m\right]A_y D_y^m + \left[I_F^m - I_B^m\right]A_z D_z^m = \left[-\beta V I_P^m + V S_P^m\right]\Delta\Omega^m \tag{13}$$

where A_x, A_y and A_z are the areas of the x-, y- and z-faces of the 3-D control volume, respectively (Fig. 1a). In Eq. (13), I with suffixes E, W, N, S, F and B designate east, west, north, south, front and back control surface average intensities, respectively. On the right-hand side of Eq. (13), $V = dx \times dy \times dz$ is the volume of the cell and I_P^m and S_P^m are the volume averaged intensity and source term at the cell center P, respectively.

In any discrete direction having index m, the two cell-surface intensities and the cell-center intensity I_P^m can be related as

$$I_P^m = \frac{I_E^m + I_W^m}{2} = \frac{I_N^m + I_S^m}{2} = \frac{I_F^m + I_B^m}{2} \tag{14}$$

While marching from the first quadrant of a 3-D enclosure for which D_x^m, D_y^m and D_z^m are all positive, from Eqs. (13) and (14), I_P^m in terms of known I_W^m, I_S^m, I_F^m and S_P^m is written as

$$I_P^m = \frac{2D_x^m A_x I_W^m + 2D_y^m A_y I_S^m + 2D_z^m A_z I_F^m + (V\Delta\Omega^m)S_P^m}{2D_x^m A_x + 2D_y^m A_y + 2D_z^m A_z + \beta V \Delta\Omega^m} \tag{15}$$

Similar equations can be derived for the situation when marching from other quadrants in which case either or both of D_x^m, D_y^m and D_z^m are negative.

In Eq. (6), incident radiation G is numerically computed from the following [29]

$$G \approx \sum_{k=1}^{M_\phi}\sum_{l=1}^{M_\theta} I^m(\theta_l^m, \phi_k^m) 2\sin\theta_l^m \sin\left(\frac{\Delta\theta}{2}\right)\Delta\phi \tag{16}$$

where M_θ and M_ϕ are the number of discrete points considered over the complete span of the polar angle ($0 \leqslant \theta \leqslant \pi$) and azimuthal angle ($0 \leqslant \phi \leqslant 2\pi$), respectively. Therefore, $M_\theta \times M_\phi$ constitute the number of discrete directions in which intensities are considered at any point.

The radiative heat fluxes in three coordinate directions are calculated from the following equations:

$$q_{R,x} \approx \sum_{k=1}^{M_\phi}\sum_{l=1}^{M_\theta} I^m(\theta_l^m, \phi_k^m)\left[\cos\phi_k^m \sin\left(\frac{\Delta\phi^m}{2}\right) \times \left(\Delta\theta - \cos 2\theta_l^m \sin(\Delta\theta)\right)\right] \tag{17a}$$

$$q_{R,y} \approx \sum_{k=1}^{M_\phi}\sum_{l=1}^{M_\theta} I^m(\theta_l^m, \phi_k^m)\left[\sin\phi_k^m \sin\left(\frac{\Delta\phi^m}{2}\right) \times \left(\Delta\theta - \cos 2\theta_l^m \sin(\Delta\theta)\right)\right] \tag{17b}$$

$$q_{R,z} \approx \sum_{k=1}^{M_\phi}\sum_{l=1}^{M_\theta} I^m(\theta_l^m, \phi_k^m)\cos\theta_l^m \sin(\theta_l^m)\sin(\Delta\theta)\Delta\phi \tag{17c}$$

While marching from any of the corners, evaluation of Eq. (15) requires knowledge of the boundary intensity. For a diffuse-gray boundary having temperature T_b and emissivity ε_b, the boundary intensity I_b is computed from

$$I_b = \frac{\varepsilon_b \sigma T_b^4}{\pi} + \left(\frac{1-\varepsilon_b}{\pi}\right)\int_{\hat{n}\cdot\hat{s}^m<0} I(\theta,\phi)(\hat{n}\cdot\hat{s}^m)\, d\Omega \tag{18}$$

Once the intensity distributions are known, radiative information $\nabla\cdot\vec{q}_R$ required for the energy equation is computed from

$$\nabla\cdot\vec{q}_R = \beta(1-\omega)\left(4\pi\frac{\sigma T^4}{\pi} - G\right) \tag{19}$$

2.2. Lattice Boltzmann Method (LBM)

The discrete Boltzmann equation with Bhatnagar–Gross–Krook (BGK) approximation is given by [25]

$$\frac{\partial f_i(\vec{r},t)}{\partial t} + \vec{e}_i\cdot\nabla f_i(\vec{r},t) = -\frac{1}{\tau}\left[f_i(\vec{r},t) - f_i^{(0)}(\vec{r},t)\right] \quad i = 0,1,2,\ldots,b \tag{20}$$

where f_i is particle distribution function at the lattice node $\vec{r}$, e_i is propagation speed in the particular direction i, τ is the relaxation time, $f_i^{(0)}$ is the equilibrium distribution function and b is the number of directions through which information propagates.

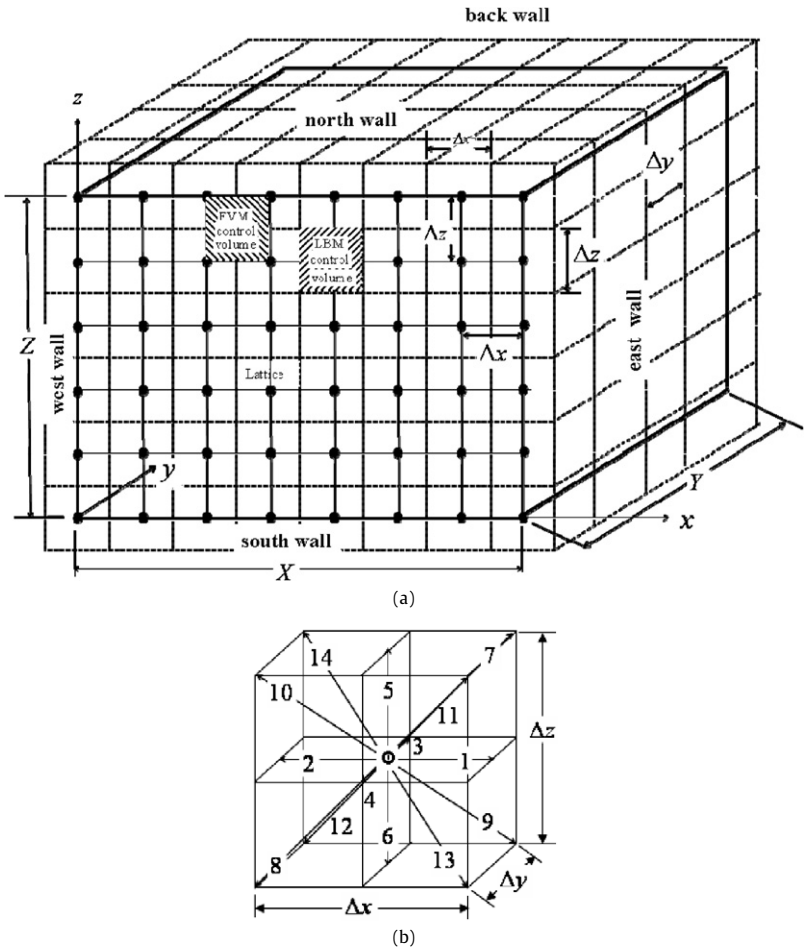

Fig. 1. (a) Arrangement of lattices and control volumes in a 3-D Cartesian geometry. (b) D3Q15 lattice in a 3-D geometry.

The relaxation time τ for the D3Q15 lattices (Fig. 1b) is given by

$$\tau = \frac{3\alpha}{|\vec{e}_i|^2} + \frac{\Delta t}{2} \tag{21}$$

where α is thermal diffusivity and Δt is time step.

For the D3Q15 lattice, the propagation speed $\vec{e}$ and corresponding weights w_i are given by

$$e_0 = (0, 0, 0)$$

$$e_{1,2} = (\pm 1, 0, 0) \cdot U$$

$$e_{3,4} = (0, \pm 1, 0) \cdot U$$

$$e_{5,6} = (0, 0, \pm 1) \cdot U$$

$$e_{7,\ldots,14} = (\pm 1, \pm 1, \pm 1) \cdot U \tag{22a}$$

$$w_0 = \frac{2}{9}, \quad w_{1,\ldots,6} = \frac{1}{9}, \quad w_{7,\ldots,14} = \frac{1}{72} \tag{22b}$$

where with uniform lattices, $U = \Delta x/\Delta t = \Delta y/\Delta t = \Delta z/\Delta t$. It is to be noted that the weights satisfy the relation $\sum_{i=1}^{b} w_i = 1$.

After discretizing Eq. (20) and considering the phase change in the presence of volumetric radiation, Eq. (20) gets modified to

$$f_i(\vec{r} + \vec{e}_i \Delta t, t + \Delta t) = f_i(\vec{r}, t) - \frac{\Delta t}{\tau}\left[f_i(\vec{r}, t) - f_i^{(0)}(\vec{r}, t)\right] - \Delta t w_i \Phi_i - \left(\frac{\Delta t}{C}\right) w_i \nabla \cdot \vec{q}_R \tag{23}$$

where

$$\Phi_i = \frac{L\rho}{C}\left[\frac{f_l(\vec{r}, t + \Delta t) - f_l(\vec{r}, t)}{\Delta t}\right] \tag{24}$$

It is to be noted that the relaxation time τ, the density ρ and the heat capacity C are different for different zones. With f_i known, temperature is obtained after summing f_i over all directions.

$$T(\vec{r}, t) = \sum_{i=0}^{b} f_i(\vec{r}, t) \tag{25}$$

To process Eq. (23), an equilibrium distribution function is required which is given by

$$f_i^{(0)}(\vec{r}, t) = w_i T(\vec{r}, t) \tag{26}$$

Eq. (23) is the desired equation to be used in the LBM that gives the same solution as that given by the energy equation (3).

3. Results and discussion

The following two cases have been considered:

- Solidification of a 3-D semitransparent medium with all boundaries at specified temperatures: Initially the 3-D cubical semitransparent participating medium (Fig. 1a) is at temperature T_0 and for time $t > 0$, its south and north boundaries are maintained at constant temperature $T_S = T_N < T_f$. The remaining four boundaries are at initial temperature $T_0 > T_f$.

- Solidification of a 3-D semitransparent medium with one of its boundaries at constant heat flux: Initially the 3-D cubical semitransparent participating medium (Fig. 1a) is initially at temperature T_0. At time $t > 0$, the constant heat flux $q_{T,S}$ is extracted from the south boundary. The north boundary is kept at constant temperature $T_N < T_f$. All other four boundaries are maintained at initial temperature $T_0 > T_f$.

The computer code for the present 3-D solidification problem has been validated against the results given in [33]. In [33], conduction-radiation problem in a 3-D cubical enclosure has been considered without any phase change. The FVM has been used to compute radiative information and also to solve the energy equation. In Fig. 2, with $\beta = 1.0$ and $\omega = 0.0$, for conduction-radiation parameter $N = 1.0$, 0.1 and 0.01, along z/Z direction at $x/X = 0.5$ and $y/Y = 0.5$ the centreline non-dimensional temperature $\theta = T/T_0$ have been compared. Results of the present work have been compared with those given in [33]. A very good agreement is observed.

For a cubical medium undergoing solidification, grid independence results are shown in Figs. 3a and 3b. With 4×8 rays,

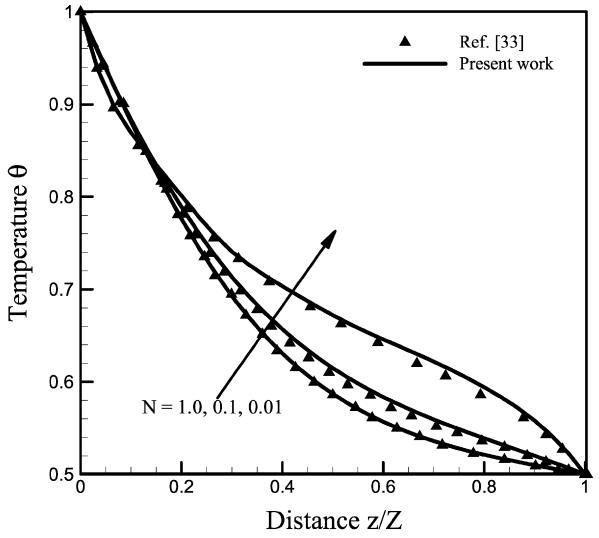

Fig. 2. Comparison of results of the present work with those of Talukdar et al. [33].

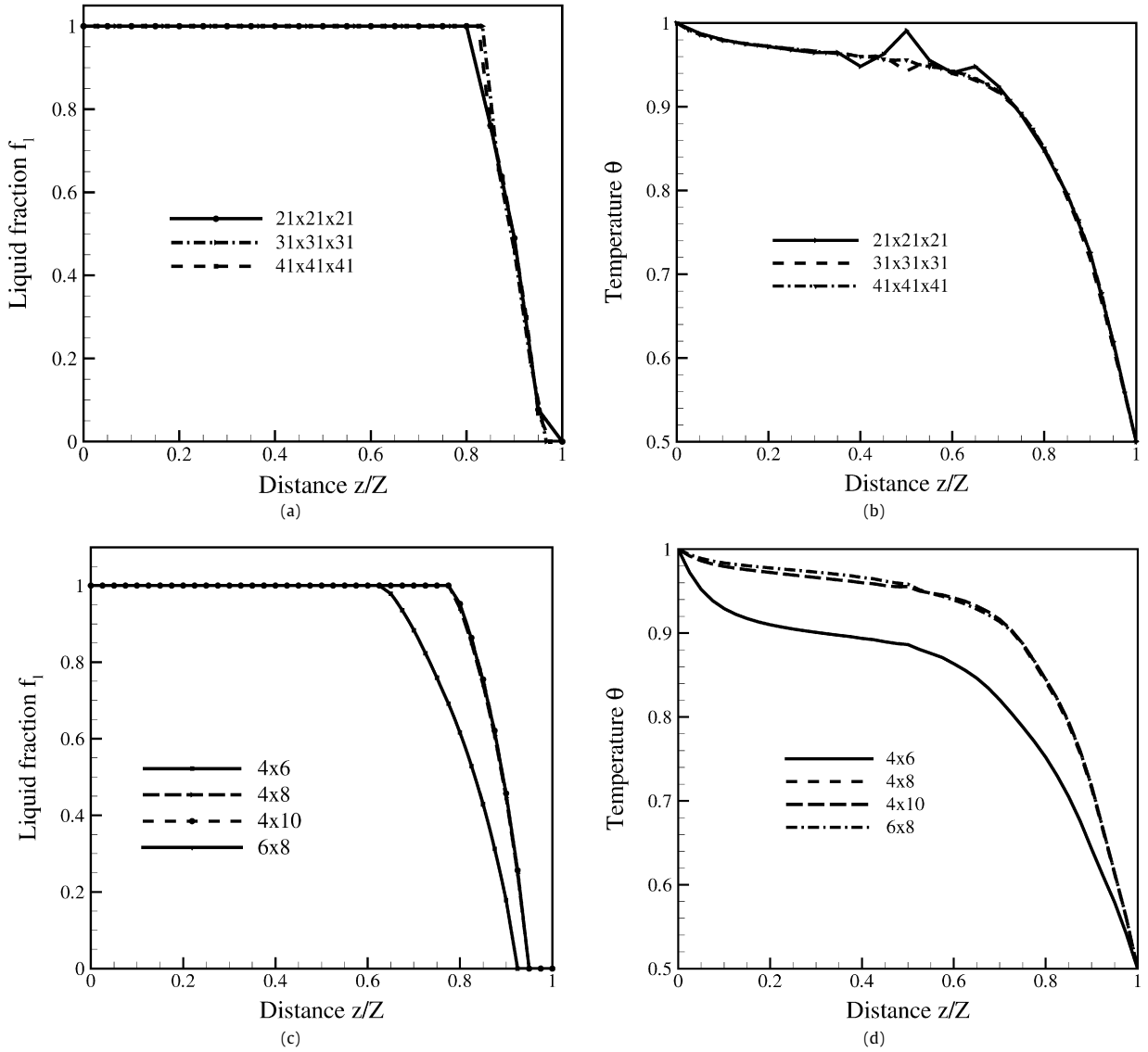

Fig. 3. Grid- and ray-independency tests: effects of number of lattices/control volumes on centre line (a) liquid fraction, (b) temperature distribution for 4×8 rays; Effects of number of rays on centerline (c) liquid fraction, (d) temperature distribution for 41×41 lattices/control volumes.

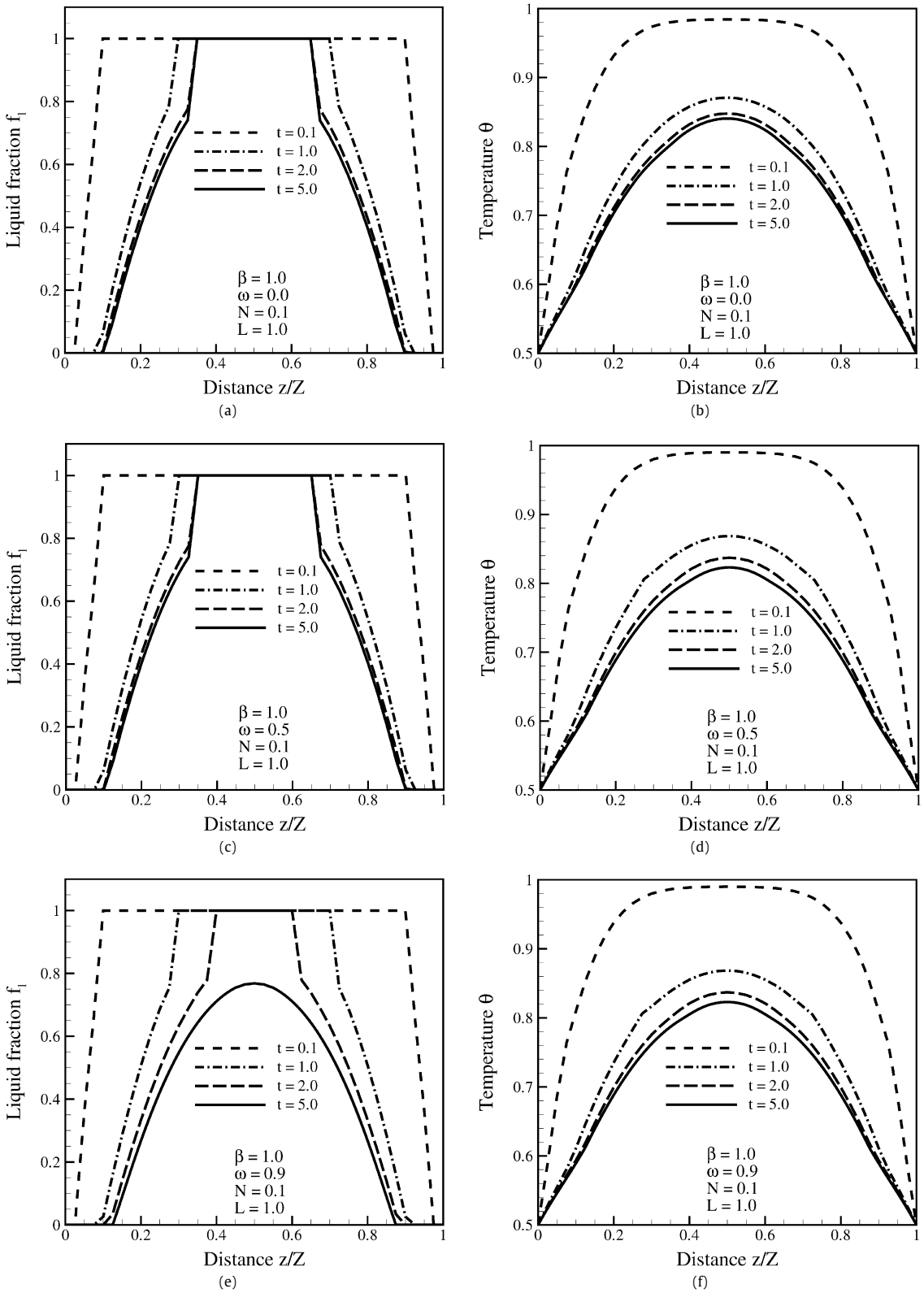

Fig. 4. Transient value of centre line ($x/X = 0.5$, $y/Y = 0.5$, z/Z) liquid fraction and temperature variations of the cubical enclosure for $\beta = 1.0$, $N = 0.1$, $L = 1.0$ and (a), (b) $\omega = 0.0$, (c), (d) $\omega = 0.5$, and (e), (f) $\omega = 0.9$.

Figs. 3a and 3b respectively show centreline liquid fraction f_l and temperature $\theta = T/T_0$ along z/Z direction at $x/X = 0.5$ and $y/Y = 0.5$ of the cubical medium for $21 \times 21 \times 21$, $31 \times 31 \times 31$ and $41 \times 41 \times 41$ lattices/control volumes. It is seen from Figs. 3a and 3b that the results of f_l have a slight variation in the mushy zone and the centreline temperature θ profiles are independent of the lattices/control volumes. It is found that $41 \times 41 \times 41$ lattices/control volumes are optimum since there is no significant improvement even for $41 \times 41 \times 41$ lattices/control volumes.

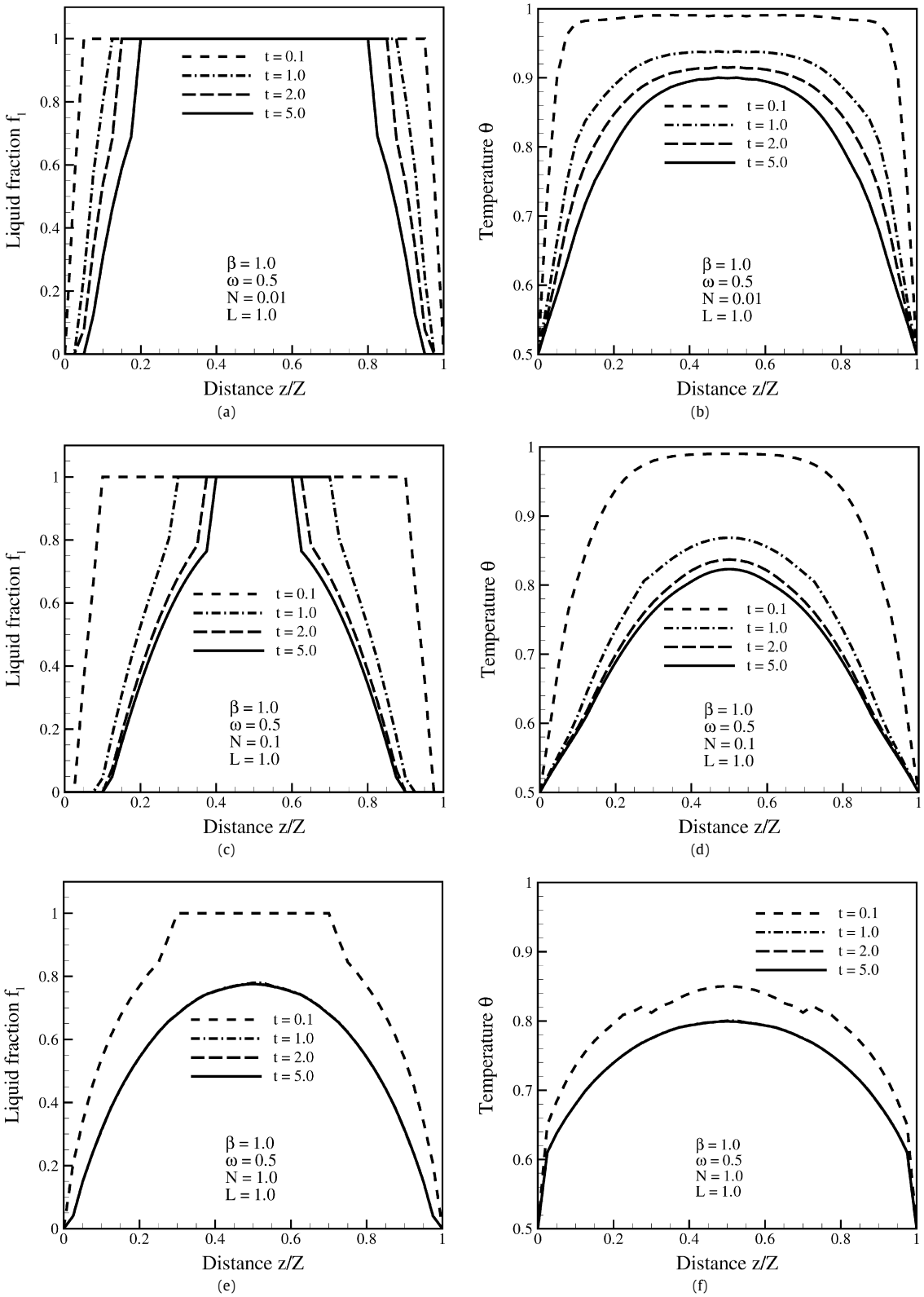

Fig. 5. Transient value of centre line ($x/X = 0.5$, $y/Y = 0.5$, z/Z) liquid fraction and temperature variations of the cubical enclosure for $\beta = 1.0$, $\omega = 0.5$, $L = 1.0$ and (a), (b) $N = 0.01$, (c), (d) $N = 0.1$, and (e), (f) $N = 1.0$.

With $41 \times 41 \times 41$ lattices/control volumes, effects of different number of rays on centerline ($x/X = 0.5$, $y/Y = 0.5$) liquid fraction f_l and the temperature θ distributions along z/Z are shown in Figs. 3c and 3d, respectively. No significance change is observed in f_l and θ distributions beyond 4×8 rays.

For the problem under consideration, all results are, therefore, presented for $41 \times 41 \times 41$ lattices/control volumes and 4×8 rays.

In present study, material properties considered are those given in [1,8]. The ratio of the thermal conductivity of materials in liquid-zone and solid-zone is $k_l/k_s = 0.6$, mushy-zone to solid-zone

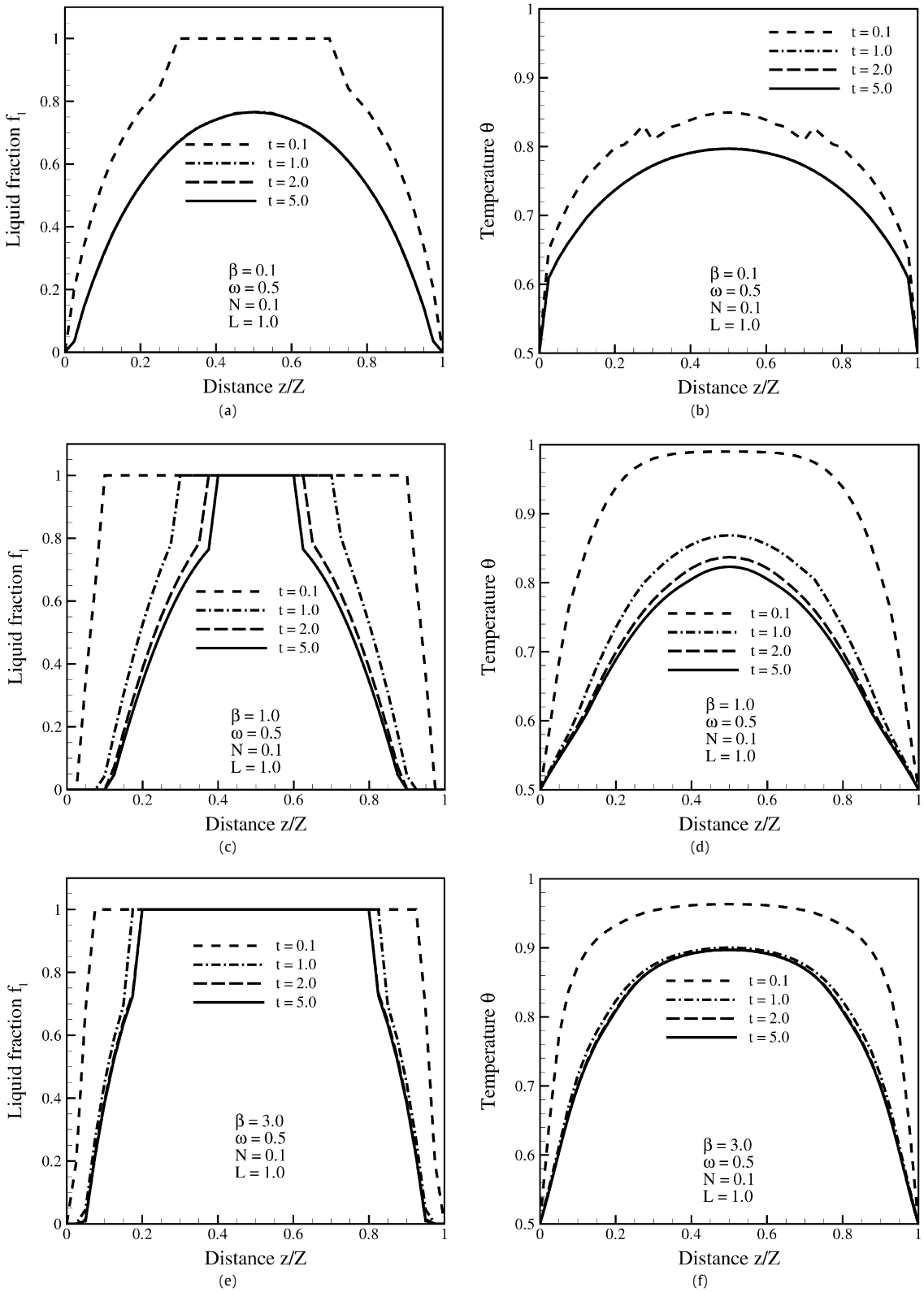

Fig. 6. Transient value of centre line ($x/X = 0.5$, $y/Y = 0.5$, z/Z) liquid fraction and temperature variations of the cubical enclosure for $\omega = 0.5$, $N = 0.1$, $L = 1.0$ and (a), (b) $\beta = 0.1$, (c), (d) $\beta = 1.0$, and (e), (f) $\beta = 3.0$.

is $k_{mz}/k_s = 0.76$, the ratio of heat capacity of liquid-zone to solid-zone is $C_l/C_s = 1.2$ and mushy-zone to solid-zone is $C_{mz}/C_s = 1.12$. The numerical values of thermal diffusivity α for the three regions are calculated from the knowledge of the above ratios. The temperatures $\theta = T/T_0$ at the solid-mushy and mushy-liquid interfaces were set at 0.6 and 0.8, respectively.

Case 1. Solidification of a 3-D semitransparent medium with all boundaries at specified temperatures.

Effects of the scattering albedo ω on liquid fraction f_l and temperature θ distributions along the centreline ($x/X = 0.5$, $y/Y = 0.5$, z/Z) are shown in Figs. 4a–4f. These results are given for the extinction coefficient $\beta = 1.0$, the conduction radiation parameter

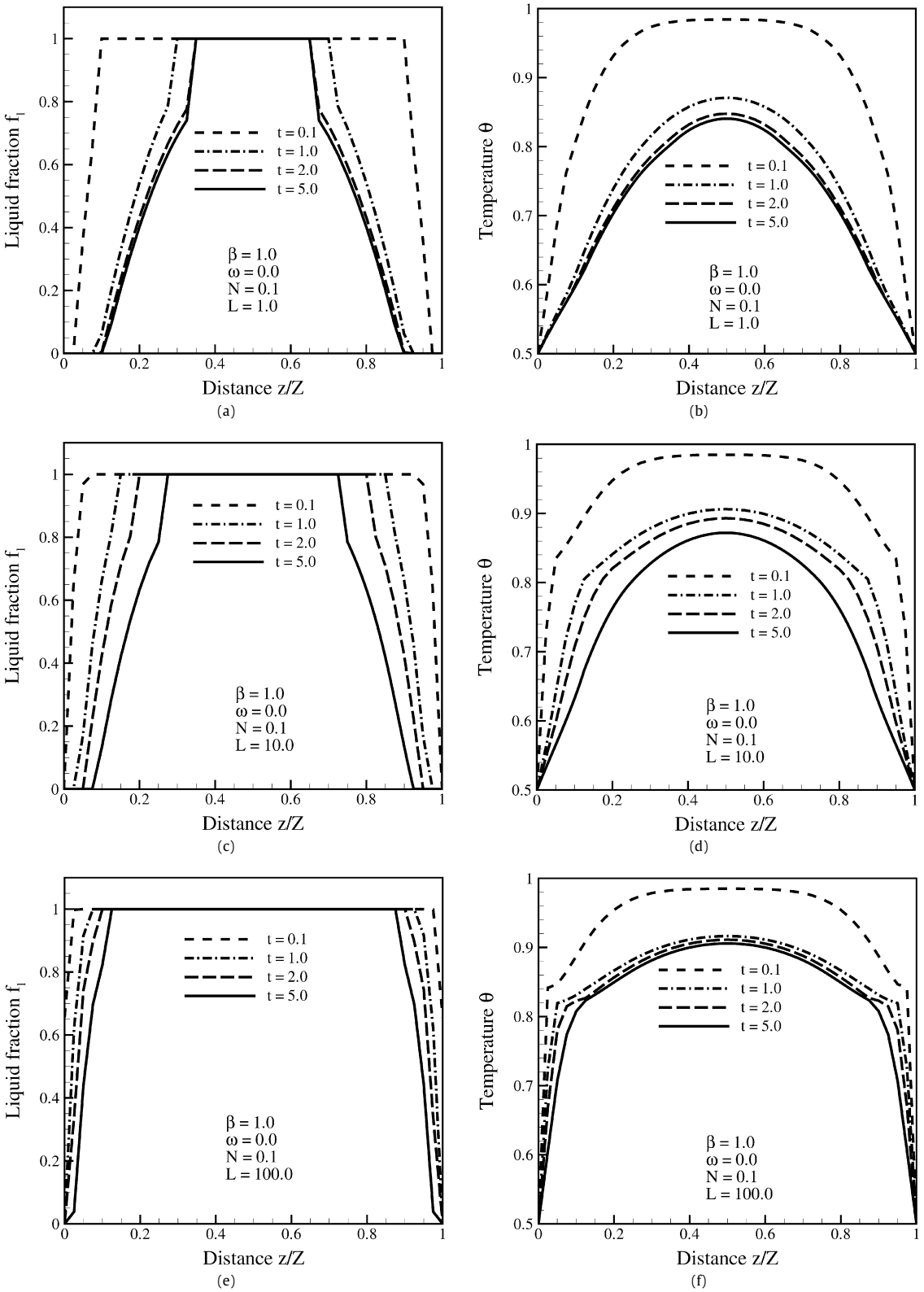

Fig. 7. Transient value of centre line ($x/X = 0.5$, $y/Y = 0.5$, z/Z) liquid fraction and temperature variations of the cubical enclosure for $\beta = 1.0$, $N = 0.1$, $\omega = 0.5$ and (a), (b) $L = 1.0$, (c), (d) $L = 10.0$, and (e), (f) $L = 100.0$.

$N = 0.1$ and the latent heat $L = 1.0$. For every value of ω, results are shown at 4 different time levels. In Figs. 4a and 4b, results are given for an absorbing-emitting medium $\omega = 0.0$. It is seen from Fig. 4a that with time t, the mushy zone thickness increases. With $\omega = 0.0$, radiation effect is more (Eq. (19)), thus in Fig. 4b, temperature gradient is more. For an absorbing, emitting and isotropically scattering medium with $\omega = 0.5$ and 0.9, f_l and θ profiles at different times are shown in Figs. 4c–4f, respectively. From Figs. 4a, 4c and 4e, it is observed that with increase in ω, thickness of the mushy-zone increases and from Figs. 4b, 4d and 4f, it is seen that

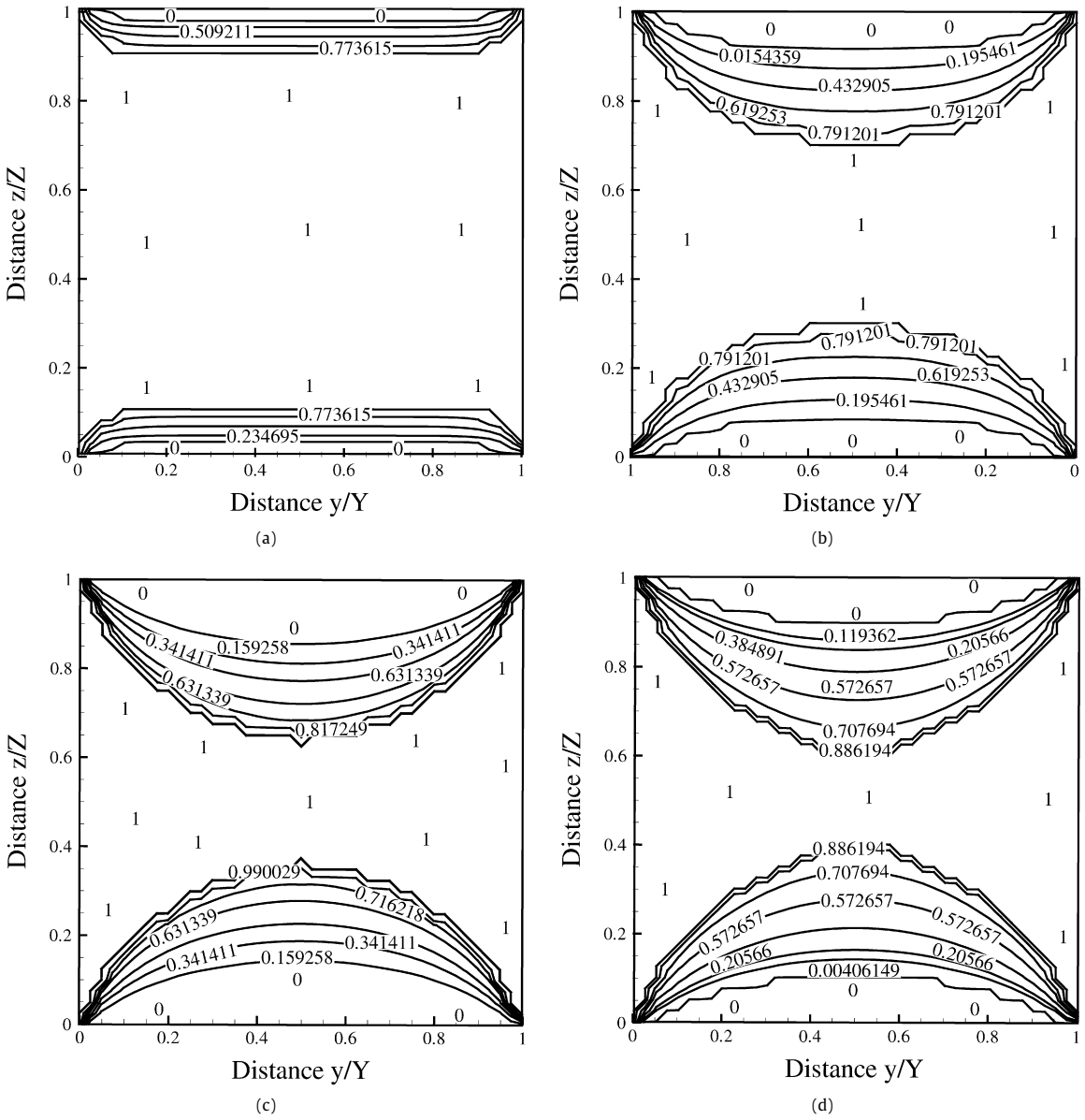

Fig. 8. Liquid fraction f_l contours at time (a) $t = 0.1$ s, (b) $t = 1.0$ s, (c) $t = 2.0$ s, (d) $t = 5.0$ s for $\beta = 1.0$, $\omega = 0.5$, $N = 0.1$, $L = 1.0$.

temperature gradient decreases. When $\omega = 0.9$, along the centerline ($x/X = 0.5$, $y/Y = 0.5$, z/Z), at time $t = 5.0$ s, no liquid-zone is observed. This is because of the fact that with increase in ω, the medium scatters more energy (Eq. (19)), and thus it is able to hold less radiation.

With $\beta = 1.0$, $\omega = 0.5$ and $L = 1.0$, effects of conduction-radiation parameter N on centerline ($x/X = 0.5$, $y/Y = 0.5$, z/Z) liquid fraction f_l and temperature θ distributions at different instants t are shown in Figs. 5a–5f. In Figs. 5a and 5b, results are given for $N = 0.01$. Here, thickness of the mushy-zone is less (Fig. 5a) and high temperature gradients are observed (Fig. 5b). $N = 0.01$ corresponds to radiation dominated case and thus the movement of the phase-front is slow. For $N = 0.1$ and $N = 1.0$, the liquid fraction f_l profiles are shown in Figs. 5c and 5e, respectively. For $N = 0.1$ and $N = 1.0$, the θ profiles are shown in Figs. 5d and 5f, respectively. The mushy zone thickness is more for higher values of N (conduction dominated situation) and its movement is also fast. In the mushy zone, the temperature gradient is less in the conduction dominated ($N = 1.0$) case. It is to be noted that in the case of conduction dominated situation ($N = 1.0$), the f_l and θ profiles do not change as time progresses from for $t = 1.0$ s to $t = 5.0$ s (Figs. 5e and 5f).

Effects of the extinction coefficient β on centerline ($x/X = 0.5$, $y/Y = 0.5$, z/Z) liquid fraction f_l and temperature θ profiles at different times are shown in Figs. 6a–6f. In this case, the other parameters are taken as $\omega = 0.0$, $N = 0.1$ and $L = 1.0$. The liquid fraction f_l profiles are shown in Figs. 6a, 6c and 6e for $\beta = 0.1$, $\beta = 1.0$ and $\beta = 3.0$, respectively. In case of a radiatively less participating medium ($\beta = 0.1$), it is found that f_l and θ profiles do not change after $t = 1.0$ s. With increase in β, the mushy-zone thickness is found to decrease. From Figs. 6b, 6d and 6f, it is observed that θ profiles become steeper with increase in β. In case of a radiatively more participating medium (higher values of β), the mushy-zone thickness is less and temperature gradient is high. The movement of phase-front is fast in case of a radiatively less participating medium ($\beta = 0.1$). This is because, in this case, radiation penetrates to a higher depth.

Effects of the latent heat L on centerline ($x/X = 0.5$, $y/Y = 0.5$, z/Z) liquid fraction f_l and temperature θ distributions at different times are shown in Fig. 7. These results are shown for $\beta = 1.0$,

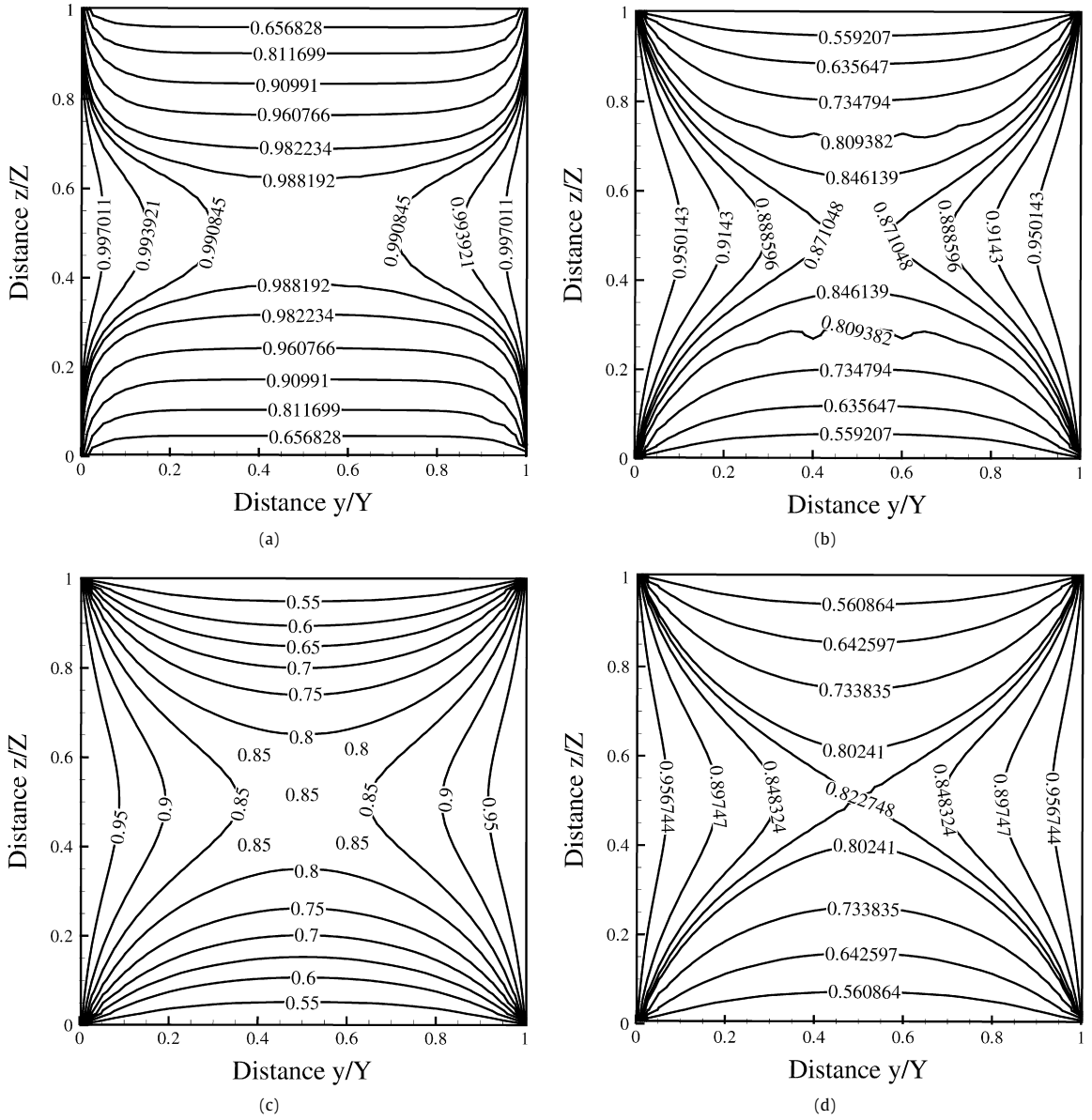

Fig. 9. Temperature θ contours at time (a) $t = 0.1$ s, (b) $t = 1.0$ s, (c) $t = 2.0$ s, (d) $t = 5.0$ s for $\beta = 1.0$, $\omega = 0.5$, $N = 0.1$, $L = 1.0$.

$\omega = 0.0$ and $N = 0.1$. For $L = 1.0$, in Figs. 7a and 7b, results are shown for liquid fraction f_l and temperature θ, respectively. For $L = 10.0$ and $L = 100.0$, f_l and θ profiles are given in Figs. 7c–7f. For a higher values of L, the mushy-zone thickness decreases and temperature gradient is steeper in the mushy-zone. This trend is attributed to the fact that when L is large, a phase change from liquid to solid requires more energy.

In Figs. 8a–8d, liquid fraction f_l contours are shown for $\beta = 1.0$, $N = 0.1$, $\omega = 0.5$ and $L = 1.0$. At four different time t levels, these contours are plotted in the y–z plane at $x/X = 0.5$. In Figs. 8a–8d, liquid fraction f_l contours are shown at time $t = 0.1$, 1.0, 2.0 and 5.0 s, respectively. The mushy-zone thickness is found to increase with time. It is observed from Figs. 8a and 8b that in the early stage, the mushy-zone grows at a faster rate but its movement becomes slow at later stages (Figs. 8c and 8d).

For $\beta = 1.0$, $N = 0.1$, $\omega = 0.5$ and $L = 1.0$, temperature θ contours in the y–z plane at $x/X = 0.5$ are shown in Figs. 9a–9d at four different time t levels. At an early stage (Fig. 9a, $t = 0.1$ s), temperature of the medium is very high. Very close to the south and the north boundaries, the temperature is less. In Fig. 9b, for at $t = 1.0$ s, it is seen that near the south and the north boundaries, temperature decrease is fast. As time elapses, temperature gradient decreases (Figs. 9c and 9d). Since the south and the north boundaries are maintained at the same temperature, which is lower than the freezing temperature T_f, the solidification starts from these boundaries and gives the symmetrical temperature profiles in the y–z plane at $x/X = 0.5$.

Case 2. Solidification of a 3-D semitransparent medium with one of its boundaries at constant heat flux.

Effects of heat flux $q_{T,S}$ extraction from south boundary on centerline ($x/X = 0.5$, $y/Y = 0.5$, z/Z) liquid fraction f_l and temperature θ profiles are shown in Figs. 10a–10f. These results are shown at four different time levels. For these results, parameters are taken as $\beta = 1.0$, $N = 0.1$, $\omega = 0.5$ and $L = 1.0$. For results in Figs. 10a and 10b, $q_{T,S} = 1.0$. $q_{T,S} = 2.0$ and 3.0 have been taken for results in Figs. 10c, 10d and 10e, 10f, respectively. It is observed from Figs. 10a, 10c and 10e, it is observed that as time elapses, thickness of the mushy-zone increases. It is further observed that with increase in the value of the extracted heat flux $q_{T,S}$, the so-

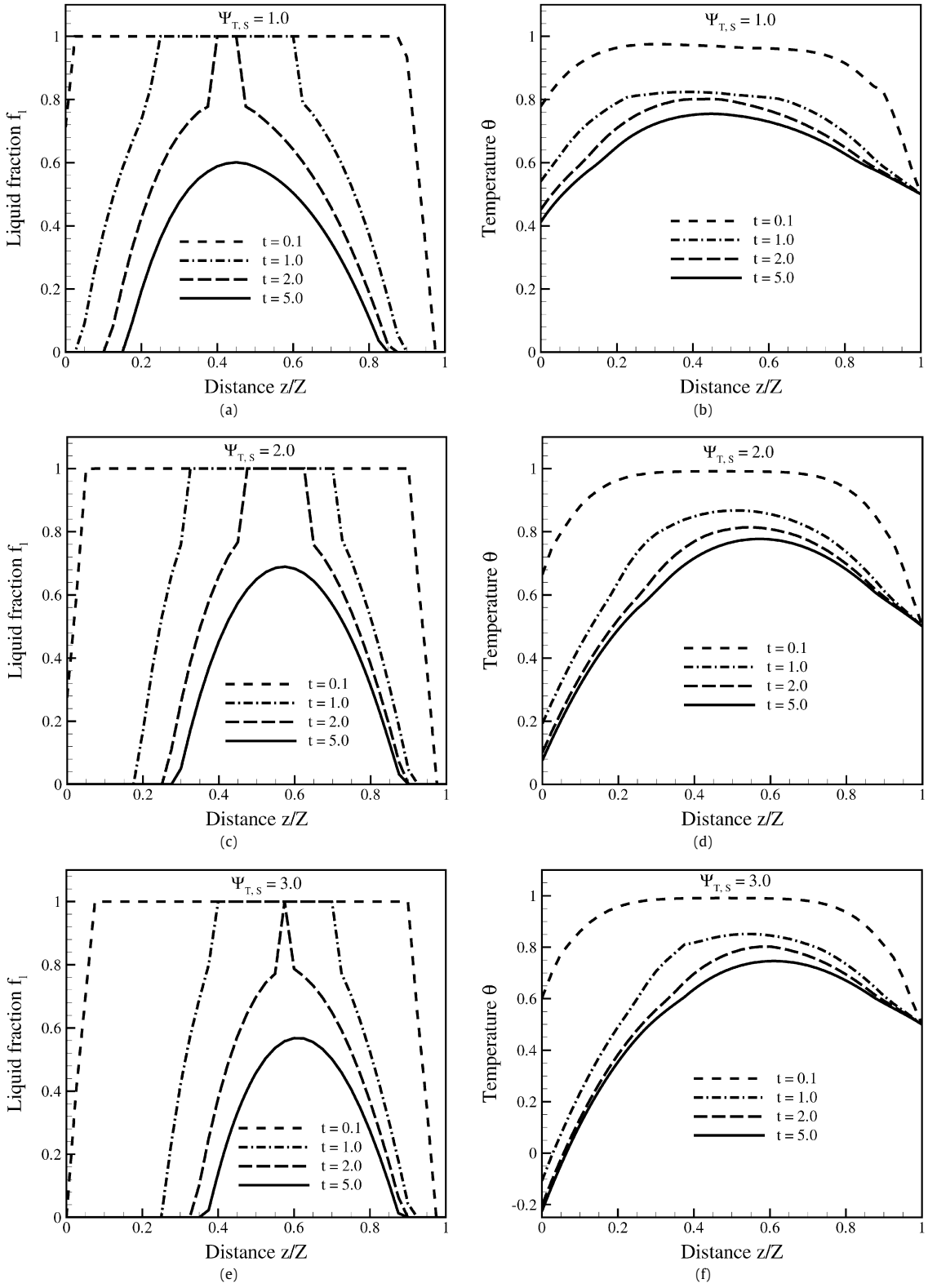

Fig. 10. Transient value of centre line ($x/X = 0.5$, $y/Y = 0.5$, z/Z) liquid fraction f_l and temperature θ profiles of the cubical enclosure for $\beta = 1.0$, $N = 0.1$, $\omega = 0.5$, $L = 1.0$ and (a), (b) $\Psi_{T,S} = 1.0$, (c), (d) $\Psi_{T,S} = 2.0$, and (e), (f) $\Psi_{T,S} = 3.0$.

lidification is more rapid. It is seen from Figs. 10b, 10d and 10f that with increase in $q_{T,S}$, temperature θ gradient increases. For a given value of $q_{T,S}$, with time, temperature θ gradient decreases. When heat extraction is more, solidification becomes fast and thus at a given instant, temperature variation in the medium will be more.

All computations in the present work were carried out with $\Delta t = 0.001$. In every case, transience was observed for 5 s. Thus, all the runs were taken for 5000 iterations. On a computer with CPU (512 MB, 2.8 GHz with hyper threading), a typical run took about 10 hours. For various cases, runs ranged from 10–12 hours.

4. Conclusions

Solidification of a 3-D cubical semitransparent absorbing and isotropically scattering medium was analyzed. An enthalpy based formulation in the LBM was used to simulate the solidification process. Radiative information was computed using the FVM. Distributions of liquid fraction and temperature were studied for the effects of the extinction coefficient, the scattering albedo, the conduction radiation parameter and the latent heat. In radiation dominated case (low value of the conduction-radiation parameter) and a strongly participating medium situation (high value of the extinction coefficient), the thickness of the mushy zone was observed to be less and its movement was slow. With increase in scattering (high value of scattering albedo), the mushy zone thickness was found to be more. A high value of the latent heat was found to yield a thinner mushy zone. Increase in heat flux extraction from the south boundary resulted in rapid solidification. With a thicker mushy zone, temperature profiles in the medium were found to be steeper.

References

[1] S.H. Co, J.E. Sunderland, Heat conduction problems with melting or freezing, J. Heat Transfer 91 (1969) 421–426.
[2] I.S. Habib, Solidification of semitransparent materials by conduction and radiation, Int. J. Heat Mass Transfer 14 (1971) 2161–2164.
[3] M. Abrams, R. Viskanta, The effects of radiative heat transfer upon the melting and solidification of semitransparent crystals, J. Heat Transfer 96 (1974) 184–190.
[4] F.O. Oruma, M.N. Ozisik, M.A. Boles, Effects of anisotropic scattering on melting and solidification of a semi-infinite semi-transparent medium, Int. J. Heat Mass Transfer 28 (1985) 441–449.
[5] V.S. Yuferev, Z. Chvoj, E.N. Kolesnikova, The effect of radiative heat transfer on morphological stability during directional solidification of a binary melt, J. Cryst. Growth 108 (1991) 367–376.
[6] Y. Shu, B.Q. Al, L. A1, K.G. Lynn, Numerical modeling of internal radiation and solidification in semitransparent melts in magnetic fields, Numer. Heat Transfer B 45 (2004) 957–976.
[7] R. Raj, A. Prasad, P.R. Parida, S.C. Mishra, Analysis of solidification of a semitransparent planar layer using the lattice Boltzmann method and the discrete transfer method, Numer. Heat Transfer A 49 (2006) 279–299.
[8] S.C. Mishra, N.C. Behera, A.K. Garg, A. Mishra, Solidification of a 2-D semitransparent medium using the lattice Boltzmann method and the finite volume method, Int. J. Heat Mass Transfer 51 (2008) 4447–4460.
[9] D. Chatterjee, S. Chakraborty, An enthalpy-based lattice Boltzmann model for diffusion dominated solid–liquid phase transformation, Phys. Lett. A 341 (2005) 320–330.
[10] S. Chakraborty, P. Dutta, Three-dimensional double-diffusive convection and macrosegregation during non-equilibrium solidification of binary mixtures, Int. J. Heat Mass Transfer 46 (2003) 2115–2134.
[11] D. Chatterjee, S. Chakraborty, A hybrid lattice Boltzmann model for solid–liquid phase transition in presence of fluid flow, Phys. Lett. A 351 (2006) 359–367.
[12] D. Chatterjee, S. Chakraborty, An enthalpy-source based lattice Boltzmann model for conduction dominated phase change of pure substances, Int. J. Thermal Sci. 47 (2008) 552–559.
[13] G. De Fabritiis, A. Mancini, D. Mansutti, S. Succi, Mesoscopic models of liquid/solid phase transitions, Int. J. Modern Phys. C 9 (1998) 1–11.
[14] W. Miller, S. Succi, D. Mansutti, Lattice Boltzmann model for anisotropic liquid–solid phase transition, Phys. Rev. Lett. 86 (2001) 3578–3581.
[15] C.C. Tseng, R. Viskanta, Melting of a semitransparent bed of particles by convection and radiation, J. Am. Ceram. Soc. 89 (2006) 2547–2554.
[16] E.M. Genies, M. Lapkowski, C. Santier, E. Vieil, Polyaniline, spectrochemistry, display and battery, Synth. Met. 18 (1987) 631–636.
[17] B. Scosati, Conducting polymers: new frontiers and prospective, Mat. Sci. Eng. 12 (1992) 369–373.
[18] V.P. Petrov, Optical and thermophysical properties of semitransparent materials in the calculation of combined radiation-conduction heat transfer, Sov. Tech. Rev. B Therm. Phys. 4 (1973) 1–79.
[19] J. Chen, A.K. Burrell, G.E. Callis, D.L. Officer, G.F. Swiegers, Preparation, characterization and biosensor application of conditioning polymers based on ferrocene substituted thiopene and terthiophene, Electrochim. Acta 47 (2002) 2715–2724.
[20] K. Gurunathan, D. Amalnerkar, D. Triovedi, Synthesis and characterization of conducting polymer composite for cathode material in rechargeable battery, Mat. Lett. 57 (2003) 1642–1648.
[21] P. Sadooghi, Transient coupled radiative and conductive heat transfer in a semitransparent layer of ceramic, J. Quant. Spectros. Radiat. Transfer 92 (2005) 403–416.
[22] X. He, S. Chen, G.D. Doolen, A novel thermal model for the lattice Boltzmann method in incompressible limit, J. Comput. Phys. 146 (1998) 282–300.
[23] H. Xi, G. Peng, S.-H. Chou, Finite-volume lattice Boltzmann schemes in two and three dimensions, Phys. Rev. E 60 (1999) 3380–3388.
[24] N. Takada, M. Misawa, A. Tomiyama, S. Fujiwara, Numerical simulation of two- and three-dimensional two-phase fluid motion by lattice Boltzmann method, Comput. Phys. Comm. 129 (2000) 233–236.
[25] S. Succi, The Lattice Boltzmann Method for Fluid Dynamics and Beyond, Oxford University Press, 2001.
[26] W.S. Jiaung, J.R. Ho, C.P. Kuo, Lattice Boltzmann method for heat conduction problem with phase change, Numer. Heat Transfer B 39 (2001) 167–187.
[27] J.R. Ho, C.-P. Kuo, W.-S. Jiaung, C.-J. Twu, Lattice Boltzmann scheme for hyperbolic heat conduction equation, Numer. Heat Transfer B 41 (2002) 591–607.
[28] J.R. Ho, C.-P. Kuo, W.-S. Jiaung, C.-J. Twu, Lattice Boltzmann scheme for hyperbolic heat conduction equation, Numer. Heat Transfer B 41 (2002) 591–607.
[29] S.C. Mishra, A. Lankadasu, Analysis of transient conduction and radiation heat transfer using the lattice Boltzmann method and the discrete transfer method, Numer. Heat Transfer A 47 (2005) 935–954.
[30] S.C. Mishra, H.K. Roy, Solving transient conduction-radiation problems using the lattice Boltzmann method and the finite volume method, J. Comput. Phys. 233 (2007) 89–107.
[31] M.F. Modest, Radiative Heat Transfer, 2nd edition, Academic Press, New York, 2003.
[32] J.C. Chai, S.V. Patankar, Finite volume method for radiation heat transfer, Adv. Numer. Heat Transfer 2 (2000) 110–135.
[33] P. Talukdar, F.V. Issendrorff, D. Trimis, C.J. Simonson, Conduction-radiation interaction in 3-D irregular enclosures using the finite volume method, Heat Mass Transfer 44 (2007) 695–704.